Carbon Dioxide Storage Capacity of Organic-Rich Shales

S.M. Kang, E. Fathi, R.J. Ambrose, I.Y. Akkutlu, and **R.F. Sigal,** The University of Oklahoma

Summary

This paper presents an experimental study on the ability of organic-rich-shale core samples to store carbon dioxide (CO_2). An apparatus has been built for precise measurements of gas pressure and volumes at constant temperature. A new analytical methodology is developed allowing interpretation of the pressure/volume data in terms of measurements of total porosity and Langmuir parameters of core plugs. The method considers pore-volume compressibility and sorption effects and allows small gas-leakage adjustments at high pressures. Total gas-storage capacity for pure CO_2 is measured at supercritical conditions as a function of pore pressure under constant reservoir-confining pressure. It is shown that, although widely known as an impermeable sedimentary rock with low porosity, organic shale has the ability to store significant amount of gas permanently because of trapping of the gas in an adsorbed state within its finely dispersed organic matter (i.e., kerogen). The latter is a nanoporous material with mainly micropores (< 2 nm) and mesopores (2–50 nm). Storage in organic-rich shale has added advantages because the organic matter acts as a molecular sieve, allowing CO_2—with linear molecular geometry—to reside in small pores that the other naturally occurring gases cannot access. In addition, the molecular-interaction energy between the organics and CO_2 molecules is different, which leads to enhanced adsorption of CO_2. Hence, affinity of shale to CO_2 is partly because of steric and thermodynamic effects similar to those of coals that are being considered for enhanced coalbed-methane recovery.

Mass-transport paths and the mechanisms of gas uptake are unlike those of coals, however. Once at the fracture/matrix interface, the injected gas faces a geomechanically strong porous medium with a dual (organic/inorganic) pore system and, therefore, has choices of path for its flow and transport into the matrix: the gas molecules (1) dissolve into the organic material and diffuse through a nanopore network and (2) enter the inorganic material and flow through a network of irregularly shaped voids. Although gas could reach the organic pores deep in the shale formation following both paths, the application of the continua approximation requires that the gas-flow system be near or beyond the percolation threshold for a consistent theoretical framework. Here, using gas permeation experiments and history matching pressure-pulse decay, we show that a large portion of the injected gas reaches the organic pores through the inorganic matrix. This is consistent with scanning-electron-microscope (SEM) images that do not show connectivity of the organic material on scales larger than tens of microns. It indicates an in-series coupling of the dual continua in shale. The inorganic matrix permeability, therefore, is predicted to be less, typically on the order of 10 nd. More importantly, although transport in the inorganic matrix is viscous (Darcy) flow, transport in the organic pores is not due to flow but mainly to molecular transport mechanisms: pore and surface diffusion.

Introduction

One of the primary considerations in subsurface sequestration of anthropogenic CO_2 is the knowledge of the gas storability of the geological formation. At a glance, a formation with a high pore volume would appear to be a good candidate for the purpose. However, this initial impression needs to be tempered because not all high-porosity formations are suitable for permanent storage of the gas. Some of them lack a suitable storage environment that will foster physical mechanisms of gas trapping. In the absence of a trapping mechanism, a free-gas cap is artificially created in the formation, which may not warrant long-term storage of the injected gas. The trapping is associated with fluid/fluid or fluid/solid interactions in porous media, such as dissolution, physical adsorption, or some homogeneous and heterogeneous reactions. Depleted oil reservoirs, for example, could be considered among the acceptable target locations. The trapping mechanism is mainly driven by absorption of the injected gas by the immobile residual oil. This is often accomplished through multiple-contact (dynamic) miscibility, which involves simultaneous phase-change and mass-transport phenomena. These reservoirs can also trap CO_2 that is not dissolved in the reservoir fluids to the extent that the reservoir seals for hydrocarbons also form a capillary seal for CO_2. Saline aquifers, on the other hand, allow aqueous-phase precipitation reactions as well as absorption by the formation water. However, the dissolved gas promotes density-driven natural convection of water and the related hydrodynamic instabilities; consequently, the injected gas could be transported and dispersed over large distances, leading to uncertainties in its fate. Coalbeds and naturally occurring gas-hydrate reservoirs have been proposed as economically feasible choices of location because the injected CO_2 not only could be sequestered in sorbed states (adsorbed on microporous coal material surfaces and absorbed into organic macromolecular openings in coal and in water) but also could participate in enhanced recovery of natural gas by an in-situ molecular swapping mechanism that promotes release and displacement of methane as a free gas. Introduction of greenhouse gases into these formations, however, is a difficult field operation because of a significant loss in well injectivity or no injectivity.

The present work is a fundamental-level investigation on gas shales as another location for subsurface CO_2 sequestration. Thermally mature organic-rich shales have proved to be prolific reservoirs for natural-gas production. In the United States, there is large production from numerous wells and an extensive pipeline structure associated with organic-shale-gas reservoirs located near major population centers, such as the Barnett, adjacent to Dallas/Fort Worth, and the Marcellus, in New York state. These shales store methane over geologic time spans both in sorbed states and as free gas. Also, much like the other shales playing the roles of a barrier or seal in a petroleum-reservoir system, they have ultralow permeability. Therefore, as the gas wells are depleted, these shales will become a natural candidate to sequester CO_2.

Shale sediments with potential for natural-gas production are generally rich in organic matter, also known as kerogen. **Table 1** shows that the total organic content (TOC) in shale could be up to 10% of the total shale weight for the North American shale-gas plays. Although this may not be perceived as a large value, the significance of the organic matter in the storage of gases in shale becomes more obvious when one considers its contribution to the total shale pore volume. In the unconventional-gas-research community, it is increasingly accepted that the organic matter is the main constituent of total pore volume, which is associated with in-situ generation and storage of natural gas. In this study, we experimentally predict an organic-pore-volume/total-pore-volume ratio up to 70% for Barnett-shale samples. The organic matter in shale could be a suitable place for CO_2 sequestration.

This paper (SPE 134583) was accepted for presentation at the SPE Annual Technical Conference and Exhibition, Florence, Italy, 20–22 September 2010, and revised for publication. Original manuscript received for review 28 June 2010. Revised manuscript received for review 28 September 2010. Paper peer approved 5 October 2010.

TABLE 1—TYPICAL TOC OF NORTH AMERICAN SHALE-GAS PLAYS*

Shale or Play	Average TOC (wt%)
Barnett	4
Marcellus	1–10
Haynesville	0-8
Horn River	3
Woodford	5

* Ambrose et al. 2010

The paper is organized as follows. At micron scale, the organic-rich gas shales have been visually investigated recently by several groups (Loucks et al. 2009; Wang and Reed 2009; Sondergeld et al. 2010). Salient results relevant to sequestration will be summarized from these petrophysical investigations. Following that, we introduce an approach that uses typical equilibrium adsorption data, assumes Langmuir monolayer adsorption, and yields effective organic pore size as an indication of organic pore space available for the storage. It is shown that the shale organics are nanoporous materials. Although they may not be suitable for storing large volumes of CO_2 as free gas, they are characterized by a large internal surface area suitable for trapping significant amounts of gas at an adsorbed state. Having small organic pores introduces new complications into the storage-capacity and transport measurements, however. The organic pore volume is a dynamic stress-dependent quantity. Next, in the light of this observation, we introduce a new methodology for the measurement of total shale porosity and gas-storage capacity where the pore volume is allowed to change as a function of pore pressure because of both adsorption/absorption and because of pore-volume compressibility. The method is based on a five-parameter nonlinear model of storability under equilibrium conditions, where the parameters will require a minimum five-stage laboratory-measurement process using the hydrocarbon gas in the reservoir or CO_2. The method will be applied to the estimation of storage with pure methane and pure CO_2. Finally, shale-gas-permeation experiments and pressure-pulse-decay measurements are performed, investigating mass-transport mechanisms in the presence of adsorption using various gases. Although pulse-decay analysis is common in the industry for the laboratory measurement of low-permeability samples, our approach is new and unconventional. It involves a simulation-based nonlinear history-matching algorithm where the new pore-scale considerations of gas shales have been incorporated into the pulse-decay analysis through forward simulation of gas flow and transport in the core plug. We predict shale-gas quantities of practical interest, such as organic pore volume, porosity, permeability, and molecular-diffusion coefficients, as a function of pore pressure. These measurements will allow us to investigate the nature of gas transport in organic-rich shale.

Pore-Scale Considerations in Organic-Rich Gas Shale

Fig. 1a shows a typical 2D focused-ion-beam/SEM (FIB/SEM) image of gas shale at micron scale. The image shows organic matter in dark gray as a finely dispersed porous material imbedded within light-gray inorganic clays. Pores are shown in black, and note that most of them are within organic islands, or kerogen pockets, that have characteristic size between 200 and 500 nm. The average size of the organic pores is typically much smaller than those we observe elsewhere in the inorganic matrix. In the next section, we present an analytical approach showing that the organic material mainly consists of micropores (pore lengths less than 2.0 nm) and mesopores (pore lengths between 2 and 50 nm), with an average pore size below 4–5 nm. Unfortunately, this is a length-scale that is too close to the molecular realm and beyond the maximum resolution of the current SEM technology. This suggests that, if one were allowed to look carefully at the fine details of the pore structure in the organics in Fig. 1, uniformly distributed micropores would have appeared, surrounding the currently visible ones, giving a sponge-like appearance to the kerogen pockets.

Ambrose et al. (2010) recently reported the results of an analysis involving hundreds of 2D images of organic shale samples, sequentially obtained using ion milling, and their recombined 3D shale segmentations. The digital segment analysis reveals kerogen pore networks. A typical network consisting of large interconnected pockets of kerogen is shown in Fig. 1b. Although the samples represent an extremely small portion of the reservoir and additional studies are currently necessary for statistical inference, the following fundamental conclusions will be made for the consideration of CO_2 storage and transport: The organic-rich-shale matrices consist of organic and inorganic materials that could be dispersed within each other or bicontinuous and, at times, intertwined; a major fraction of the total porosity within the system is associated with the kerogen network, and therefore much of the gas-storage capacity within shale is predominantly associated with the organic fraction of the rock matrix. In the following pages, we will take advantage of these observations and develop a new conceptual shale-matrix model that involves a porous medium with dual (organic/inorganic) -porosity continua. The approach will allow us to quantify and measure total gas storage and transport in organic-rich shale samples.

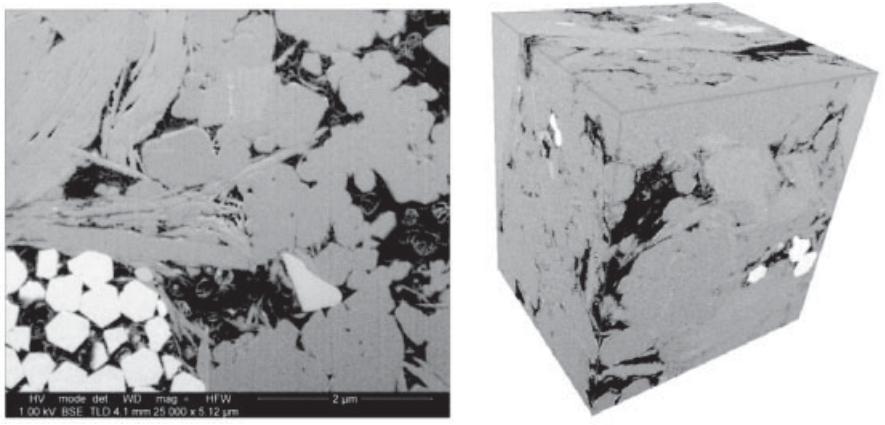

(a) (b)

Fig. 1—(a) 2D backscatter FIB/SEM image of a gas-shale sample. (b) 3D FIB/SEM shale segmentation. The shale segmentation size is 4 µm high, 5 µm wide, and 4 µm deep.

Effective Organic Pore Size. An effective-pore-size-estimation approach considers that gas adsorption takes place only on the organic pore walls in the kerogen pockets. The approach is based on the premise that an estimate of total surface area of the organic material in shale can be realized if a method is developed whereby the amount of adsorbed gas corresponding to monolayer coverage can be determined. Physically, the monolayer approach may not mean much when pores are so small, although a simple surface-science concept could help us illustrate the potential features of organic shale. For simplicity, we consider that all of the pores in the organics will have the same shape: either spherical or cylindrical because both shapes will be investigated. We used methane for the analysis, and the shale has the physical characteristics shown in **Table 2.** First, the total volume available for gas sorption must be calculated. It is assumed that the pores containing water will not have any surfaces where gas adsorption can occur and that the volume of gas that can dissolve in the clay-bound water is negligible. Hence, total shale gas pore volume per bulk volume is equal to $\phi\,(1-S_w)$. Consider that only ε_{k0} fraction of this total gas pore volume is associated with the organics; hence, the gas pore volume in the organics is $\varepsilon_{k0}\,\phi\,(1-S_w)$. The expression can be written in terms of volumes (cm^3) as follows: $[\text{mass/density}]_{\text{rock}}\,\varepsilon_{k0}\,\phi\,(1-S_w)$. Thus, using the values in Table 2, the gas-filled organic pore space for 1.0 ton of shale rock is equal to

$$\left(\frac{1\text{ ton}}{2.5\text{g/cm}^3}\right)\times\left(\frac{907{,}184.75\text{ g}}{\text{ton}}\right)\times 0.5\times 0.05\times(1-0.35)=5{,}896.7\text{ cm}^3.$$

The number of lbm mol in 1.0 scf of gas is

$$\frac{n}{V}=\frac{P_{\text{std}}}{RT_{\text{std}}}=\frac{14.69\text{ psi}}{\left(10.7316\ \frac{\text{scf psi}}{^\circ\text{R lbm mol}}\right)\times(60+459.67)^\circ\text{R}}=2.6340\times10^{-3}\ \frac{\text{lbm mol}}{\text{scf}}.$$

Therefore, the number of methane molecules in 50 scf/ton of gas (Langmuir volume) would be

$$(50.0\text{ scf})\times\left(2.6340\times10^{-3}\ \frac{\text{lbm mol}}{\text{scf}}\right)\times\left(453.5924\,\frac{\text{g}}{\text{lbm}}\right)\times\left(6.0221\times10^{23}\,\frac{\text{molecules}}{\text{g mol}}\right)=3.5976\times10^{25}\text{molecules}.$$

If one adsorbed methane molecule covers 0.16 nm^2 (Anderson and Pratt 1985), assuming monolayer coverage, we can estimate the total area covered by this number of methane molecules as

$$3.5976\times10^{25}\text{molecules}\times\frac{0.16\text{ nm}^2}{\text{molecule}}=5.7562\times10^{24}\text{nm}^2.$$

This is a significant value, indicating that the organic pores have relatively large internal surface area. We can use the ratio of volume to surface area to calculate the radius the molecules needed to cover for a uniform size sphere and cylinder. In the case of a cylindrical pore, we will assume that it is a cylinder without any flat ends so only the curved surface area will be calculated. For a sphere, the volume is $V=4\pi r^3/3$ and surface area is $A_s=4\pi r^2$. Hence, for the spherical pore, the volume/surface-area ratio would be $V/A_s=(4\pi r^3/3)/(4\pi r^2)=r/3$. Using similar arguments, it could be shown that the ratio for a cylindrical pore is equal to $r/2$. Next, we calculate the effective pore sizes corresponding to spherical and cylindrical geometries using the gas-filled organic pore volume of 5.8967×10^{24} nm^3 (or 5,896.7 cm^3):

$$r_{\text{sphere}}=3\left(\frac{V}{A_s}\right)=3\left(\frac{5.8967\times10^{24}\text{ nm}^3}{5.7562\times10^{24}\text{ nm}^2}\right)\cong 3.0\text{ nm}.$$

$$r_{\text{cylinder}}=2\left(\frac{V}{A_s}\right)=2\left(\frac{5.8967\times10^{24}\text{ nm}^3}{5.7562\times10^{24}\text{ nm}^2}\right)\cong 2.0\text{ nm}.$$

Table 3 shows the estimated values of spherical and cylindrical pore radii in the organics as a function of ε_{k0}. Assuming slit-type pore geometry, Schettler et al. (1989) estimated an average pore diameter of 5.5 nm for Devonian shales using the Brunauer-Emmett-Teller multilayer-adsorption isotherm method. This is a same-order-of-magnitude value. On the basis of the calculations, it can be argued that a significant portion of the organic pores are small (less than 4–6 nm) and, therefore, may not be accessible with the resolution of the SEM image shown in Fig. 1. These small organic pores, with their large surface area, are an ideal place for trapping gas in an adsorbed state and for its long-term storage. However, they make the measurements and analyses of gas storage and transport somewhat complicated because, at that length scale

- The thickness of the adsorption layer becomes comparable to the organic pore size. Under thermodynamic equilibrium (no flux of mass or energy), some of the gas molecules inside the organic pore are closer and, therefore, under stronger influence of the pore walls. These molecules have limited mobility and relatively low kinetic energy. They participate in the formation of a dense (liquid-like) adsorption layer that covers internal surfaces of the pore walls; see **Fig. 2a.** Next to the adsorption layer, we typically observe phase-transition layers where the molecules are constantly being adsorbed and desorbed under equilibrium. The molecules in phase transition are relatively less dense and more mobile with some kinetic energy, although they are under somewhat reduced influence of the walls. The rest of the gas molecules are at the central portion of the pore (if any space is left), and they are not under the influence of pore walls. They are the free-gas molecules, with a density equal to the fluid bulk density in the absence of pore walls. They mainly interact among themselves and with the gas molecules in phase transition. In the case of methane adsorption in a 3.6-nm-thick organic slit pore shown in Fig. 2, in total $2\times0.37=0.74$ nm of space next to the walls will be occupied by the adsorption layer, thus leaving only 3.6–0.74 = 2.86-nm-thick pore space available for the phase-transition molecules and

TABLE 2—SHALE PARAMETERS FOR EFFECTIVE-PORE-SIZE CALCULATIONS

Parameter	Symbol	Value
Total porosity	ϕ	5%
Organic/total pore volume ratio	ε_k	0.5
Water saturation	S_w	35%
Bulk density	ρ	2.5 g/cm^3
Langmuir volume (methane)	V_L	50 scf/ton

TABLE 3—ESTIMATED ORGANIC PORE RADII FOR VARYING ε_{k0} VALUES

Fraction of Porosity in Organic (ε_{k0})	Spherical Pore Radius, r_{sphere} (nm)	Cylindrical Pore Radius, r_{cylinder} (nm)
0.1	0.61	0.41
0.2	1.23	0.82
0.3	1.84	1.23
0.4	2.46	1.64
0.5	3.07	2.05
0.6	3.69	2.46
0.7	4.30	2.87
0.8	4.92	3.28
0.9	5.53	3.69
1	6.15	4.10

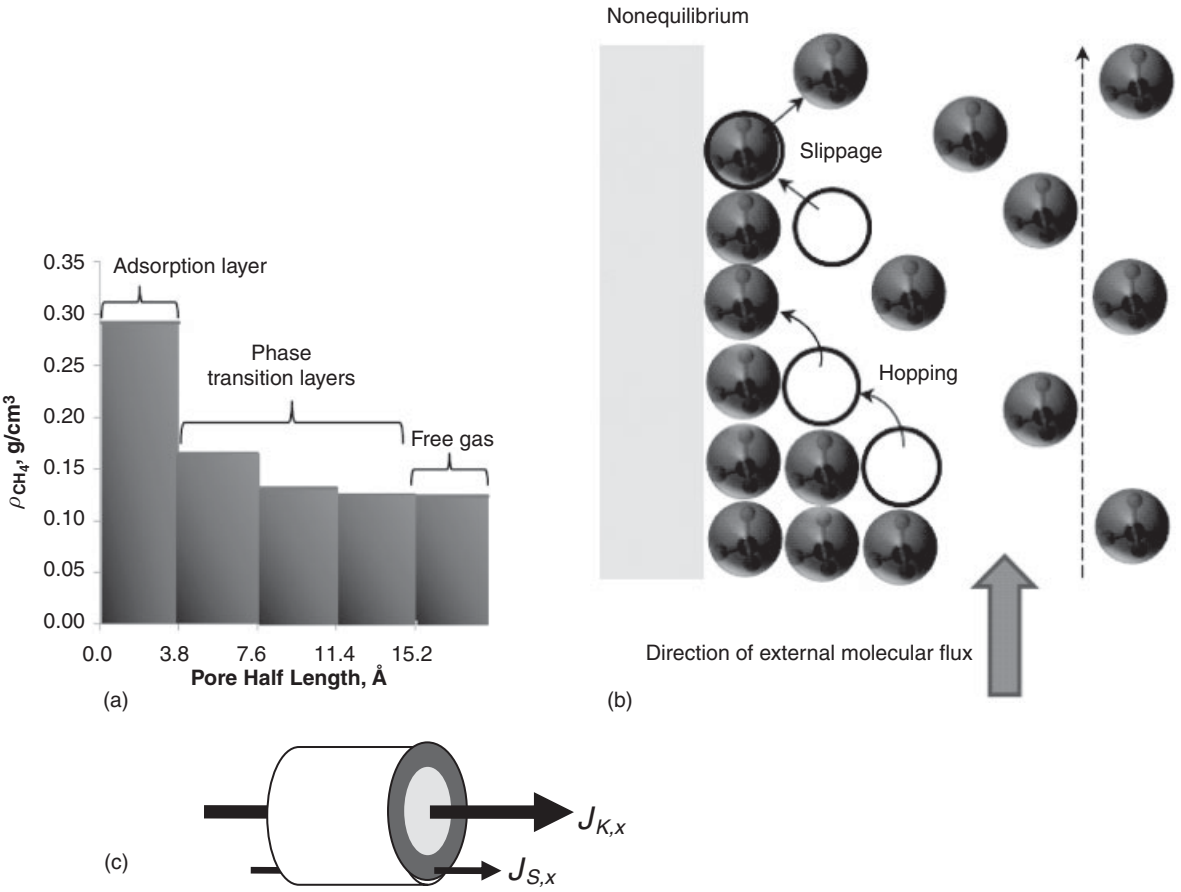

Fig. 2—(a) Molecular layer density for methane at 176°F (80°C) across the half-length of a 3.74-nm organic slit pore. Results obtained using equilibrium molecular dynamics simulation carried out in the canonical ensemble. The estimated pore pressure is approximately 2,000 psi. (b) Schematic representation of gas slippage and hopping mechanisms of molecular transport. (c) Schematic of gas mass transport in organic nanopores. The arrows represent diffusive mass fluxes of the free-gas phase (thick arrow) and the adsorbed phase (thin arrow) in the *x* direction. $J_{K,x}$ and $J_{S,x}$ are the contributions of free-gas pore diffusion and adsorbed-phase surface diffusion, respectively.

for the free-gas molecules. Density structure of gas molecules in small organic pores and its effect on shale-gas in-place estimations have been studied recently by our group; see Ambrose et al. (2010).

- The mean free path of gas molecules (i.e., average distance gas molecules travel between two successive collisions) becomes comparable to the available pore space. Consequently, the free-gas molecules interact vigorously with the molecules in phase transition and with those that make up the adsorption layer and pore wall, compared with the level of interaction the free-gas molecules have among themselves at the central portion of the pore. When thermodynamic equilibrium is perturbed because of an externally applied molecular flux, for example, these amplified interactions may lead to kinetic effect that causes streaming of the gas molecules—in particular, those in phase transition. This is the occurrence of the so-called slippage effect (or molecular streaming) in the organic pore. It can cause the collapse of laminar-flow (parabolic) -velocity profile with zero velocity at the wall. Consequently, the free-gas mass transport would show deviations from Darcy's law and would be represented better with molecular (pore) diffusion. A useful dimensionless parameter in the literature to determine the changes in flow regime of a gas system is the Knudsen number (N_{Kn}). This number is the ratio of the molecular mean free path to the pore length scale. When $N_{Kn} > 0.1$, the kinetic effect becomes dominant by the wall in the phase-transition region. Further discussion on the flow regimes can be found in Roy et al. (2003). In **Fig. 3,** we consider methane existence in organic pore volume with characteristic pore length varying between 2 and 10 nm and estimate the N_{Kn} for varying pore pressures. The values inside the ellipse (typical initial shale-gas-reservoir conditions) indicate that the gas mass transport in the organics should be in the transitional slippage-flow regime. This means that the assumption of Darcy flow is invalid in the organic pores in shale. Therefore, a new approach is necessary for modeling the gas mass transport, which will incorporate non-Darcy transport of the free-gas molecules.

- Adsorbed-phase transport could be another important mass-transfer mechanism. Fig. 2c shows the free-gas and adsorbed-phase components of total mass flux in the organic micro- and mesopore. Under the influence of an external flux, some of the molecules in the adsorbed-phase and those in phase transition can overcome the local interactions with the wall and develop a hopping mechanism. (Much like drifting of a tumbleweed or tree leaves on the ground under the influence of a mild wind.) This transport mechanism, also known as surface diffusion, is not important if it takes place in a large pore with an almost infinite number of free-gas molecules; but, if the discussion is on nanopores with a large surface area, it may easily contribute to the total mass flux and, hence, enhance the kinetic effect by the pore walls. Let us reconsider the layers of molecules indicating nonuniform structure (damped oscillation) in methane density in a 3.6-nm organic pore in Fig. 2. It is not difficult to imagine that the molecular layers corresponding to free gas would not develop and all of the existing molecules would be either adsorbed or under the influence of pore walls if the pore size were less then 2×1.08 = 2.16 nm. Then, the only transport mechanism during the gas release from or uptake by the pore would be because of surface diffusion. We note that, although they both take place in the phase-transition region, surface diffusion is a different transport mechanism than the slippage; at a given pressure and temperature, surface diffusion is driven by gradients in adsorbed-phase density, whereas slippage is driven by the pore size.

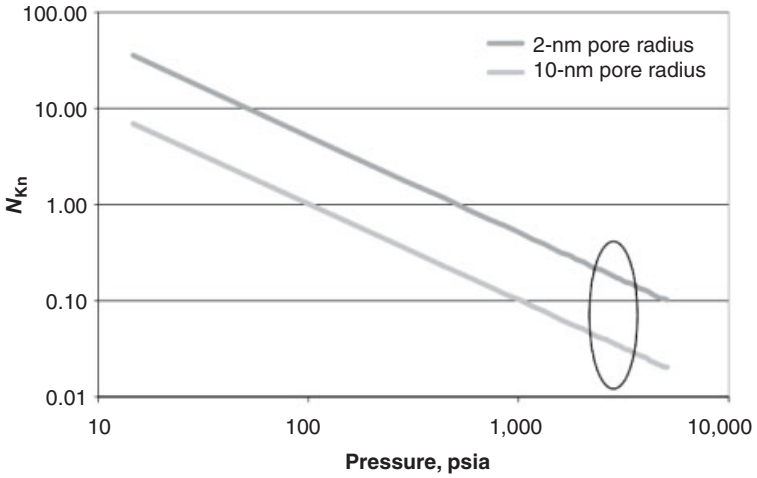

Fig. 3—Knudsen number vs. pore pressure for pore-throat radii calculated from the Langmuir isotherm at reservoir temperature of 188°F.

• The assumption of continuum-fluid mechanics may become questionable—in particular, in the micropores. A 2.86-nm pore can, at most, include only seven methane molecules in a row across the pore space. Similarly, approximately 30 methane molecules would fit in a 10-nm organic pore. Hence, the number of molecules is limited inside the organic pores, which may not allow the assumption of a representative elementary volume for the fluid (i.e., the classical fluid-particle concept of fluid mechanics) with average intensive properties, such as density and viscosity.

In this work, these pore-scale considerations will be part of the gas-storage and -transport measurements. Gas-storage measurements do not necessarily require the assumption of continuum, although the transport calculations do. Our group has other investigations based on noncontinuum approaches (e.g., molecular modeling and molecular/continuum multiscale modeling), although they are discussed elsewhere; see Diaz-Campos et al. (2009) and Ambrose et al. (2010). During the measurements at varying pore pressures, the organic pore volume available for the free gas will be adjusted for the isothermal pore compressibility effect (effective stress) and also for the presence of an adsorption layer. During transport calculations, we will differentiate free-gas and adsorbed-phase diffusive transport in the organics from gas flow in inorganic matrix and in fractures using a separate transport mechanism for each. In the organics, diffusion of the adsorbed phase accounts for surface diffusion effects of molecules in phase transition, whereas diffusion of free molecules represents transport in the pore space and slippage in the phase-transition region.

Interpretation of Organic Pore Diffusion. Consider flux of free-gas molecules across the available organic pore space in the direction parallel to its inlet and outlet ends. The net free-gas mass flux is proportional to the difference in gas number densities n_1 and n_2 at the two ends: $J_K = wc(n_2 - n_1)$, where w is a dimensionless probability factor and c is the mean molecular speed. The mean molecular speed could be estimated from the kinetic theory of gases using $c = \sqrt{[8RT/(\pi M)]}$, where M is the gram molecular weight, T is the absolute temperature, and R is the universal gas constant (Roy et al. 2003). The probability factor is dependent on the geometry of the pore and requires knowledge of the appropriate scattering law. Considering diffusive scattering and simple geometry, such as a capillary with a length L and radius r, the value of w for the condition $L >> r$ is equal to $2/3(r/L)$. Substituting these expressions into the flux equation so that it gives mass flux along the axis of a relatively long capillary pore and writing in differential form using the convention that the molecules move from high to low concentration of molecules, we obtain

$$J_{K,x} = \frac{-2r}{3}\sqrt{\frac{8RT}{\pi M}}\left(\frac{\mathrm{d}n}{\mathrm{d}x}\right). \quad \ldots\ldots\ldots\ldots\ldots\ldots\ldots\ldots\ldots\ldots (1)$$

Equivalently, this expression can be reformulated in terms of moles of concentration C rather than molecular concentration:

$$J_{K,x} = \frac{-2r}{3}\sqrt{\frac{8RT}{\pi M}}\left(\frac{\mathrm{d}C}{\mathrm{d}x}\right). \quad \ldots\ldots\ldots\ldots\ldots\ldots\ldots\ldots\ldots\ldots (2)$$

By analogy to Fickian gas diffusion, we now define a molecular-diffusion coefficient for transport in the capillary as

$$D_{K,\mathrm{capillary}} = \frac{2r}{3}\sqrt{\frac{8RT}{\pi M}}. \quad \ldots\ldots\ldots\ldots\ldots\ldots\ldots\ldots\ldots\ldots (3)$$

Thus, the diffusion coefficient is proportional to the effective (adsorption layer-corrected) pore radius and the mean molecular velocity. One can relatively easily obtain typical values to compare with the experimentally obtained organic pore diffusion coefficient. For the purpose, we consider a 1.5-nm cylindrical pore and perform the calculations at our laboratory conditions:

$$D_{K,\mathrm{capillary}} = \frac{2r}{3}\sqrt{\frac{8RT}{\pi M}} = \frac{2\times\left(1.5\times10^{-9}\,\mathrm{m}\right)}{3} \times\sqrt{\frac{8\times\left(8.3145\,\frac{\mathrm{kg\ m^2}}{\mathrm{s^2K\ mol}}\right)\times\left(298.15\ \mathrm{K}\right)}{3.1416\times\left(16.042\times10^{-3}\,\frac{\mathrm{kg}}{\mathrm{mol}}\right)}} = 6.3\times10^{-7}\,\frac{\mathrm{m^2}}{\mathrm{s}} = 6.3\times10^{-3}\,\frac{\mathrm{cm^2}}{\mathrm{s}}.$$

One would expect this estimate to be somewhat larger than the experimentally obtained molecular diffusivity because the measurement is the outcome of an expression derived for a single capillary pore. Typically, the two can be roughly related through the porosity/tortuosity ratio as

$$D_K = \left(\frac{\varepsilon_k}{\varepsilon_{\mathrm{TOC}}}\right)\left(\frac{\phi}{\tau^2}\right)D_{K,\mathrm{capillary}}, \quad \ldots\ldots\ldots\ldots\ldots\ldots\ldots\ldots (4)$$

where $\varepsilon_{\mathrm{TOC}}$ is the kerogen/total-volume ratio and τ is tortuosity. Because it cannot be measured directly, there exists uncertainty in the values of tortuosity of nanoporous materials. Values between 1.5 and 8 have been reported by Wei et al. (2007) and Busch et al. (2008). If the kerogen porosity (the first parenthesis term on the right-hand side of Eq. 4 multiplied with ϕ) is 20%, and a kerogen

tortuosity of 3.0–6.0 is assumed, one would expect that the organic pore-diffusion coefficient measured using pressure-pulse decay D_K should be on the order of 10^{-5} cm^2/s (i.e., two orders of magnitude smaller). In addition, the adsorbed-phase transport can be captured similarly using Fick's law:

$$J_{S,x} = -D_S \left(\frac{\mathrm{d}C_\mu}{\mathrm{d}x} \right), \quad (5)$$

where C_μ is the adsorbed-phase amount in terms of moles per solid organic volume and D_S is the porosity- and tortuosity-corrected surface diffusivity. Typically, for C_μ, we would expect one-order-of-magnitude-smaller values then the free-gas amount C, although its gradient could vary and be relatively large during the production and sequestration operations.

When evaluating the capacity of a shale reservoir to store CO_2, an essential first step is to evaluate the total porosity and how much gas per unit weight (scf/ton) the porous material of the reservoir can store. In general, this storage capacity is a function of the porous-material properties, the reservoir pore pressure, and the temperature. When multiple storage mechanisms are present, it is difficult to characterize the total porosity and storage. First, we explain a multistage gas-uptake process that allows determination of the total storage capacity and total porosity as a function of pressure and temperature and the parsing of the storage into the various storage mechanisms. This measurement can also be taken under in-situ subsurface conditions.

Measurement of Shale-Gas-Storage Capacity

For a shale sample, total porosity is defined as the volume of fluids (i.e., liquid and free gas, not including adsorbed or absorbed gas) contained in the sample. Hence, the storage capacity of shale should be divided up into the sorbed component and the pore-volume component. In this work, an isothermal multistep gas-uptake process measures the storage capacity. The minimum number of steps required is discussed later.

Fig. 4 shows the basic components needed for the measurement. For temperature control, or to make measurements at reservoir conditions, the apparatus can be enclosed in an oven to provide a constant high-temperature environment. Currently, we have two different storability-measurement implementations in the laboratory, one in an environmental chamber and one that operates at ambient temperature in the laboratory. The apparatus consists of a pressure vessel that contains the core sample to be tested along with a dead volume, Volume 2; a gas reservoir, Volume 1; a valve, Valve 2, to separate the reservoir volume from the sample container; a gas source, typically a pressure tank; as valves, Valve 1, to isolate the rest of the system from the gas tank; and pressure gauges. Not shown are pumps to raise the gas from the bottle pressure to the needed reservoir pore pressure and the pump and plumbing to provide confining pressure on the sample. The pressure vessel is plumbed so that the sample can be kept at a confining pressure that corresponds to the confining stress that the sample is exposed to in the reservoir. During the measurements, the confining pressure is always kept greater than the pore pressure.

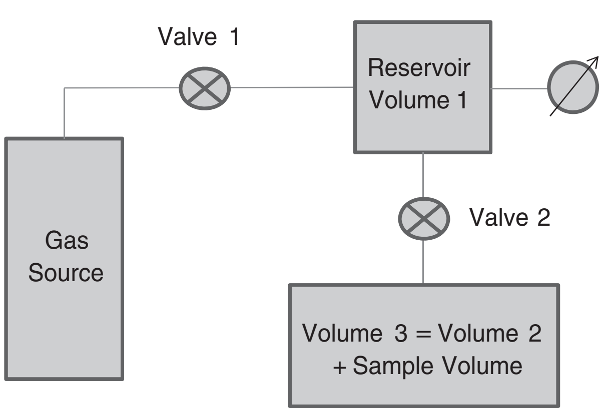

Fig. 4—Diagram of gas-storage-capacity measurement method.

The storability measurement is a multistage measurement. Each stage starts with Valve 2 closed. To start, Volume 1 is raised to a pressure P_1, and then Valve 1 is closed. The sample and dead Volume 2 are at an initial starting pressure P_2. The test consists of opening Valve 2 and recording the pressure as a function of time until it has stabilized at a new pressure P_f. The pressure-decay curve can be used to obtain the transport coefficients. The test can be run with P_1 less than P_2 (for the gas-release measurements) or P_1 greater than P_2 (for the gas-uptake measurements). In the first case, the decrease in storability with decrease in pressure is measured; and, in the second case, the increase in storability is measured.

For the second case, the analysis of a given stage proceeds as follows. The moles of gas n_1 in Volume 1, V_1, at pressure P_1 is given by

$$n_1 = P_1 V_1 / (z_1 RT), \quad (6)$$

where R is the universal gas constant, T is the absolute temperature, and z_1 is the correction factor that accounts for deviation from the ideal-gas law. The correction factor depends on temperature, pressure, and the type of gas. Numerous tables and programs exist that provide accurate values of z_1. Similarly, the moles of gas contained in V_2 initially are given by

$$n_2 = P_2 V_2 / (z_2 RT). \quad (7)$$

After Valve 2 is opened and the pressure has stabilized at P_f, the moles in V_1 and V_2 are given by

$$n_{1f} = P_f V_1 / (z_f RT)$$

and

$$n_{2f} = P_f V_2 / (z_f RT). \quad (8)$$

Mass balance requires that the decrease of moles of gas in V_1, Δn_1, is equal to the increase in moles of gas in V_2, Δn_2, plus the increase in moles of gas stored in the organic pores of the shale sample Δn_s. From the previous equations,

$$\Delta n_1 = \frac{V_1}{RT} \left(\frac{P_1}{z_1} - \frac{P_f}{z_f} \right),$$

$$\Delta n_2 = \frac{V_2}{RT} \left(\frac{P_f}{z_f} - \frac{P_2}{z_2} \right),$$

and

$$\Delta n_s = \Delta n_1 - \Delta n_2. \quad (9)$$

The additional moles of gas Δn_s stored in the sample provide the increase in storability as a function of the change in pressure. When this process is iterated over multiple steps, it provides the storability as a function of pore pressure. This is the basic information needed to characterize the reservoir and is an essential input into simulations that model the way gas will be produced from the reservoir or be sequestered in it. It should be noted that, because there can be hysteresis in the storability curves, both the increasing and decreasing storability cases may need to be measured.

To separate the storage in the rock system into the adsorbed/absorbed component and the component stored as free gas in the pore space, a model of the storage mechanisms needs to be used. The moles of gas n_{sp} stored in the sample pore space V_p in terms of the sample pore pressure P_s (P_s equals P_2 or P_f) satisfies the gas law. Therefore,

$$n_{sp} = P_s V_p / (z_s RT)$$

and

$$\Delta n_{sp} = \left(\frac{V_{pf} P_f}{z_f} - \frac{V_{p2} P_2}{z_2} \right) \Big/ RT. \quad \ldots\ldots\ldots\ldots\ldots\ldots\ldots\ldots (10)$$

In general, V_p is a function of the pore pressure and the gas type. As we will see, it may not be a single-valued function. The dependence of V_p on pressure needs to be included in the model and will be discussed after the discussion of the adsorption/absorption term. V_{p2} and V_{pf} are the pore volumes at pressures P_2 and P_f, respectively.

For both the shale-gas and the coalbed-methane cases, the amount of gas adsorbed/absorbed by the rock matrix is generally assumed to be described by a Langmuir isotherm. It is known that this is only an approximation and other more-exact models could be used to model the adsorption/absorption component of the storage. For the Langmuir model, all the nonfree gas is assumed to be adsorbed. The Langmuir isotherm is parameterized by two quantities, the total moles of adsorbed gas at infinite pore pressure $S_{a\max}$ and the Langmuir pressure P_L.

The Langmuir equation gives the adsorbed gas storage S_a as a function of the pore pressure P as

$$S_a = \frac{S_{a\max}\left(P/P_L\right)}{1+P/P_L}, \quad \ldots\ldots\ldots\ldots\ldots\ldots\ldots\ldots (11)$$

so that Δn_{sa} is given by

$$\Delta n_{sa} = S_{a\max}\left[\frac{P_f/P_L}{1+\left(P_f/P_L\right)} - \frac{P_2/P_L}{1+\left(P_2/P_L\right)} \right]. \quad \ldots\ldots\ldots\ldots\ldots (12)$$

and

$$\Delta n_s = \Delta n_a + \Delta n_{sp}.$$

The pore volume can change as a function of pressure because of both adsorption/absorption and because of pore-volume compressibility. Adsorption can affect pore volume by the adsorbed molecules occupying pore space that otherwise would be occupied by the free gas or by the adsorbed gas closing off pore throats so gas cannot get through to the larger pore. Absorption can cause the matrix to swell or, by swelling, to close off access to pores. The effects would look very similar for both adsorption and absorption. Using the Langmuir model associates all the pore-volume changes with adsorption. The Langmuir model can be used to calculate the pore-volume loss because of adsorbed gas. This calculation does not account explicitly for pore-blockage effects, but, to the extent that a Langmuir isotherm successfully fits the gas adsorption, it is implicitly including these effects. In the Langmuir equation, the term $(P/P_L)/(1+P/P_L)$ represents the fraction of the moles adsorbed at any pressure. If $V_{a\max}$ represents the maximum adsorbed-gas volume and V_a the adsorbed-gas volume at any pressure, then, assuming Langmuir adsorption,

$$V_a = \frac{V_{a\max}\left(P/P_L\right)}{1+P/P_L}. \quad \ldots\ldots\ldots\ldots\ldots\ldots\ldots\ldots (13)$$

If V_{p0} is the pore volume at zero pore pressure, then the decrease in V_p at pressure P because of adsorption is given by $V_{p0}-V_{a\max}\,(P/P_L)/(1+P/P_L)$. The decrease in V_p in each stage is

$$\Delta V_{pa} = -V_{a\max}\left[\frac{P_f/P_L}{1+\left(P_f/P_L\right)} - \frac{P_2/P_L}{1+\left(P_2/P_L\right)} \right]. \quad \ldots\ldots\ldots\ldots (14)$$

If the molar density of the adsorbed gas $\rho_{\text{ads max}}$ is known, then

$$V_{a\max} = S_{a\max}/\rho_{\text{ads max}}. \quad \ldots\ldots\ldots\ldots\ldots\ldots\ldots\ldots (15)$$

The last consideration is accounting for pore-volume compressibility. Over the pressure ranges applicable, this should be a small effect with values typically on the order of 10^{-6}. It can be determined in two ways, as part of the multistage measurement process using the adsorbed gas or as a separate process using helium, which is not adsorbed (so only a simple two-stage process needs to be performed). In either case, the pore-volume compressibility is defined by C_p so that the volume increase because of increasing pore pressure is given by

$$\Delta V_{pp} = C_p V_{p0}\,(P_f - P_2). \quad \ldots\ldots\ldots\ldots\ldots\ldots\ldots\ldots (16)$$

The total change in pore volume going from pore pressure P_2 to P_f is given by

$$\Delta V_p = \Delta V_{pp} + \Delta V_{pa}, \quad \ldots\ldots\ldots\ldots\ldots\ldots\ldots\ldots (17)$$

so that

$$V_{pf} = V_{p2} + \Delta V_p. \quad \ldots\ldots\ldots\ldots\ldots\ldots\ldots\ldots (18)$$

Here, the second-order effect of C_p being dependent on pore pressure is ignored. This model of storability has five parameters to determine, $S_{a\max}$, $V_{a\max}$, P_L, V_{p0}, and C_p. Simultaneous estimation of these quantities will require, at a minimum, a five-stage measurement process if they are all determined by measurements using the hydrocarbon gas in the reservoir or CO_2. Measurements with helium could be used to determine C_p and an approximate value for V_{p0}, assuming the density of the adsorbed-state gas is constant, and then the measurements could be reduced to two-stage measurements. The second option is experimentally easier but would not provide any test of the model assumptions. Combining the second option with a few detailed multistage measurements to obtain model-independent storability to test against the model might prove to be a cost-effective option.

Multiscale Characterization and Measurement of Shale-Gas-Transport Mechanisms

Our arguments based on the indirect laboratory observations (SEM images and storage-capacity measurements) suggest that a flow model for shale gas should include dispersed organic porous material within the inorganic matrix. A conceptual model showing the organic- and inorganic-material distribution in shale is given in **Fig. 5.** Note that, compared to coal, the main difference in shale-gas production is that, before reaching the fractures, a large portion of shale gas in place should be transported first inside the kerogen network imbedded in the matrix. It should be noted that a large contrast in length scales exists between gas flowing in the organic pores, outside of them in the matrix, and in the fractures. This requires a multicontinuum modeling approach involving separate but coupled hydraulic components of the porous medium, where each component (organic, inorganic, and fracture)

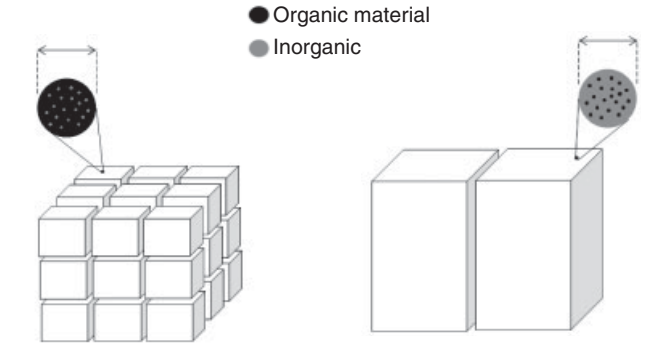

Fig. 5—Distributions of the organic and inorganic materials in coal and shale.

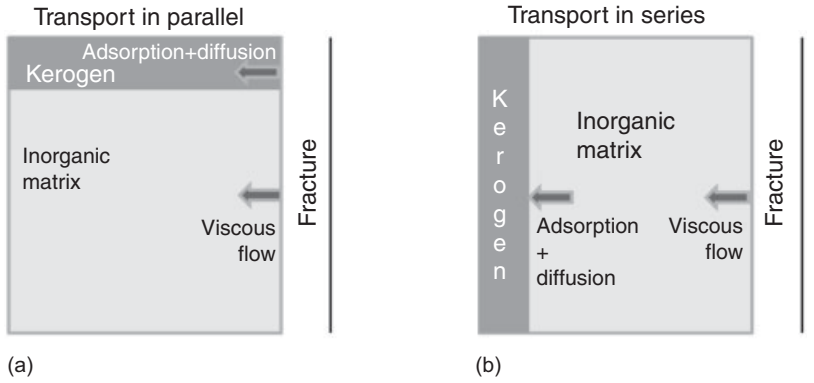

Fig. 6—Conceptual multicontinuum models for gas flow and transport in organic-rich shale during sequestration.

is distributed continuously in space and holds the fundamental porous-medium conditions specified by Bear and Bachmat (1991). Multicontinuum models can be identified by the number of components characterizing the hydraulic behavior of the system and the type of coupling and mass-exchange terms between the components. The interaction between the components, defined by finite mass-exchange terms, affects the overall transport behavior of the system significantly, while a single-continuum approach neglects this important effect. There are three different types of coupling between the components: parallel, series, and selective coupling. In parallel coupling, all specified continua are coupled with one another directly, while, in the series coupling, they are connected in the order of hydraulic conductivity (Lee and Tan 1987). In organic-rich-shale-gas reservoirs, multicontinuum could be defined, at the least, by two matrix continua (i.e., organic and inorganic, along with a fracture continuum).

In the Effective Organic Pore Size subsection, we argued that the gas mass transport in the organics is transitional slippage with adsorbed-phase surface-diffusion effects (i.e., non-Darcy). Modeling of such transitional flow regimes in the presence of adsorption is not straightforward, however. Here, following the work by Fathi and Akkutlu (2009, in press), we investigate gas-transport behavior in the kerogen by experimentally quantifying the pore and surface diffusion coefficients D_K and D_S, respectively. Pore diffusion is the mechanism of transport for the free-gas molecules occupying the available pore space, whereas surface diffusion is the mechanism of transport for the adsorbed-phase near the internal surfaces of the kerogen. During the production, gas in the kerogen pore network is eventually released to the relatively larger pores, voids, microfractures, and cracks in the inorganic matrix or directly into the nonuniform fracture network shown in Fig. 5b. In its new environment, the mechanism of its transport is primarily viscous (Darcy) flow and, because of limited surface area, the adsorbed amount is considered negligible. In the case of CO_2 sequestration, the same arguments are valid, although in the opposite transport direction (i.e., from the fractures deep into the inorganic shale matrix and into the kerogen). **Fig. 6** shows two conceptual models of shale-gas flow and transport that are considered in this study for methane production and CO_2 sequestration. In Fig. 6a, parallel coupling is shown where organic and inorganic continua are coupled directly with fractures. In Fig. 6b, all three continua are coupled in series (i.e., fracture → inorganic → organic). We used these conceptual models during the development of a mathematical formulation (a group of coupled partial-differential equations) describing the mechanisms of gas storage and transport. The formulation is used to simulate gas-permeation experiments using organic-rich shale core plugs. Later, the developed simulators are used in the experimental investigation of multiscale characterization of transport phenomena in organic-rich shales. Further discussion on the modeling and simulation of shale-gas flow can be found in Fathi (2010).

Measurements of Transport Coefficients—Unsteady Gas-Permeation Experiments. Steady-state methods for the measurements of permeability and diffusivity of shale are difficult to implement because of very low mass fluxes and the extremely long time needed to reach the steady-state condition. Therefore, transient methods such as pressure-pulse-decay experiments have been used for the measurements. This method is much faster in comparison to the conventional methods and can be used to measure permeability valuse as low as 10^{-9} md (Brace et al. 1968; Ning 1992; Finsterle and Persoff 1997; Jones 1997). In this method, a small perturbation is introduced to a shale/gas system under thermodynamic equilibrium by rapidly changing the downstream (or upstream) pressure, typically by an approximate 10% of the equilibrium pressure. Consequently, small pressure gradients are generated across the sample, leading to transport of gas across the core plug. During the gas permeation, decline in the upstream or downstream pressure is measured to extract transport properties of the shale using an analytical or numerical inversion method.

Results

Table 4 shows results from the models that fit the measured storage data for helium, CO_2, and methane with two organic-rich shale samples, Sample 21 and Sample 23. These samples are selected because TOC and mineralogy were known. Because, in the initial measurement stage, the CO_2 passes through a pressure where it can form a liquid phase, there is considerably more uncertainty in the model fits to the measured storage data. Note the estimated V_{p0} values. The values are quite different for Sample 23, giving 5.38, 3.95, and 2.89% porosity for the gases, respectively. The model fits to the experimental data are not unique. Assuming that all reasonable fits to the data have the properties of this fit, the variations indicate that methane molecules with spherical molecular geometry cannot have access to some of the micropores that CO_2 molecules with linear molecular geometry have access to, and the CO_2 molecules cannot have access to some of the micropores that the small helium molecules can access. In essence, the organic material of Sample 23 acts as a molecular sieve for fluids used during measurements; see **Fig. 7.** Although this effect creates uncertainties during the storage-capacity measurements for Sample 23, in general, it points to an important CO_2-sequestration quality for the shale-gas formations. It suggests that a large fraction of the injected CO_2 can be stored in small pores in which the other naturally occurring gases, such as methane and nitrogen, cannot be stored. Compared to methane, for example, CO_2 can access an additional $100 \times (0.4771-0.345)/0.345 = 38.3\%$ of the organic pore volume when injected into Sample 23 under the same conditions. The molecular sieving becomes a secondary effect in the case of Sample 21, however. In this case, methane and CO_2 have access to the same pore space, whereas helium can penetrate into an additional 7.7% organic-micropore volume.

As the consequence of changes in the estimated values of the pore volume V_{p0}, the predicted gas-sorption parameters in Table 4 are quite different. Effect on the Langmuir adsorption isotherm is shown in **Fig. 8.** Note that, because the pore-volume estimation for Sample 21 is consistent, the predicted methane and CO_2 isotherms

TABLE 4—MEASURED GAS-STORAGE CAPACITY FOR THE ORGANIC-RICH SHALE SAMPLES USING VARIOUS GASES

		Sample 21			Sample 23		
		He	CO_2	CH_4	He	CO_2	CH_4
V_{p0} (cc)		0.42	0.39	0.39	0.65	0.48	0.35
C_p (psi^{-1})		5.416×10^{-6}	5.416×10^{-6}	5.416×10^{-6}	7.05×10^{-6}	7.05×10^{-6}	7.05×10^{-6}
$P_{L,\,CH4}$ (psi)	using $V_{po,He}$			3,232			1,000
	using $V_{po,CH4}$			1,800			2,502
$V_{amax,\,CH4}$ (cm^3)	using $V_{po,He}$			0.4193			0.4056
	using $V_{po,CH4}$			0.1962			0.1423
$S_{amax,\,CH4}$ (mol)	using $V_{po,He}$			0.0072			0.0021
	using $V_{po,CH4}$			0.0049			0.0041
$\rho_{ads,\,CH4}$ (mol/cm^3)	using $V_{po,He}$			0.017			0.005
	using $V_{po,CH4}$			0.025			0.029
$P_{L,CO2}$ (psi)	using $V_{po,He}$		500			655	
	using $V_{po,CH4}$		500			2610	
	using $V_{po,CO2}$		500			1410	
$V_{amax,CO2}$ (cm^3)	using $V_{po,He}$		0.4118			0.4300	
	using $V_{po,CH4}$		0.3850			0.3200	
	using $V_{po,CO2}$		0.3850			0.3400	
$S_{amax,\,CO2}$ (mol)	using $V_{po,He}$		0.0240			0.0280	
	using $V_{po,CH4}$		0.0237			0.0211	
	using $V_{po,CO2}$		0.062			0.0220	
$\rho_{ads,\,CO2}$ (mol/cm^3)						0.065	

appear distinctly in Fig. 8a. The isotherms for the other sample are shown in Fig. 8b. Indeed, methane isotherms show that the gas stored as an adsorbed phase is significantly larger when the pore volume obtained using helium is included in the analysis. The contrast is even larger in the case of CO_2. These results indicate the importance of fluid type used for the adsorption analysis. In the rest of the paper, we show only the storage and transport results for a particular fluid using a sample pore volume measured with that fluid.

Modeled total gas storage is given in **Figs. 9 and 10.** The adsorbed-gas and free-gas amounts stored are shown in Fig. 9a for Sample 21 and in Fig. 9b for Sample 23. Clearly, most of the injected CO_2 is stored in an adsorbed state. For example, at 2,500 psia and for Sample 21, the ratio of adsorbed to free CO_2 is approximately 13:1. For Sample 23, that ratio drops to 13:5, although the total amount stored is nearly doubled. Hence, the measurements reveal that the samples have larger adsorption capacity for CO_2 at any given pore pressure. For both samples, the total CO_2-gas-storage capacity is 4 times greater than the total methane-gas-storage capacity at 2,500 psia. Such a large contrast in methane and CO_2 storage is important for sequestration, although it cannot be explained by the molecular-sieving arguments related to the organics of certain types of samples. It can be explained only by changes in the fluid's internal energy with the changes in the fluid type. Indeed, the molecular-interaction energies (both among the gas molecules and between the organic pore wall and gas molecules) are different, which leads to significantly enhanced adsorption in the case of CO_2. Molecular-level investigation further comparing adsorption of fluids and their mixtures in kerogen in the small organic pores under reservoir conditions is currently necessary.

Results indicate that adsorption is the dominant mechanism during the CO_2 storage in organic-rich shale. This may also be the case for methane, although the dominance is not as amplified and distinct as in the case of CO_2; see Fig. 10. At 2,500 psia, the ratio

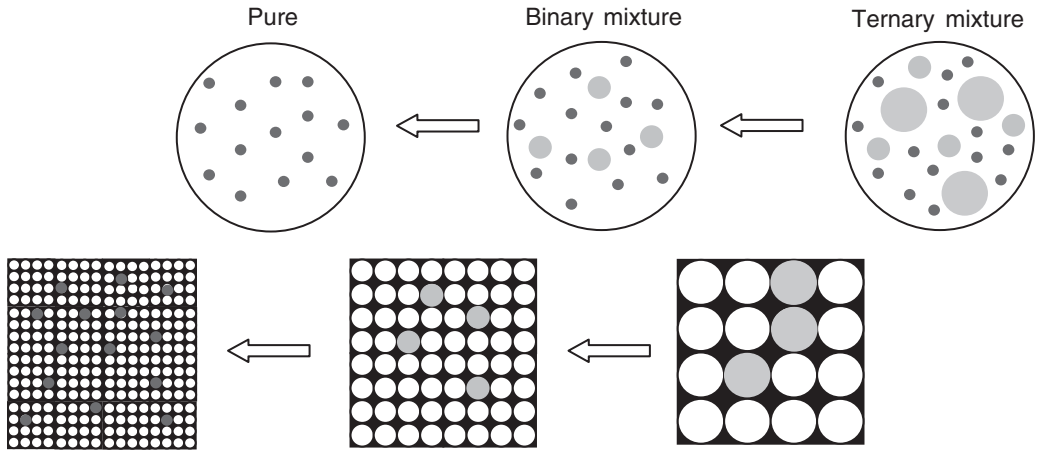

Fig. 7—Schematic of molecular sieving of gases in kerogen.

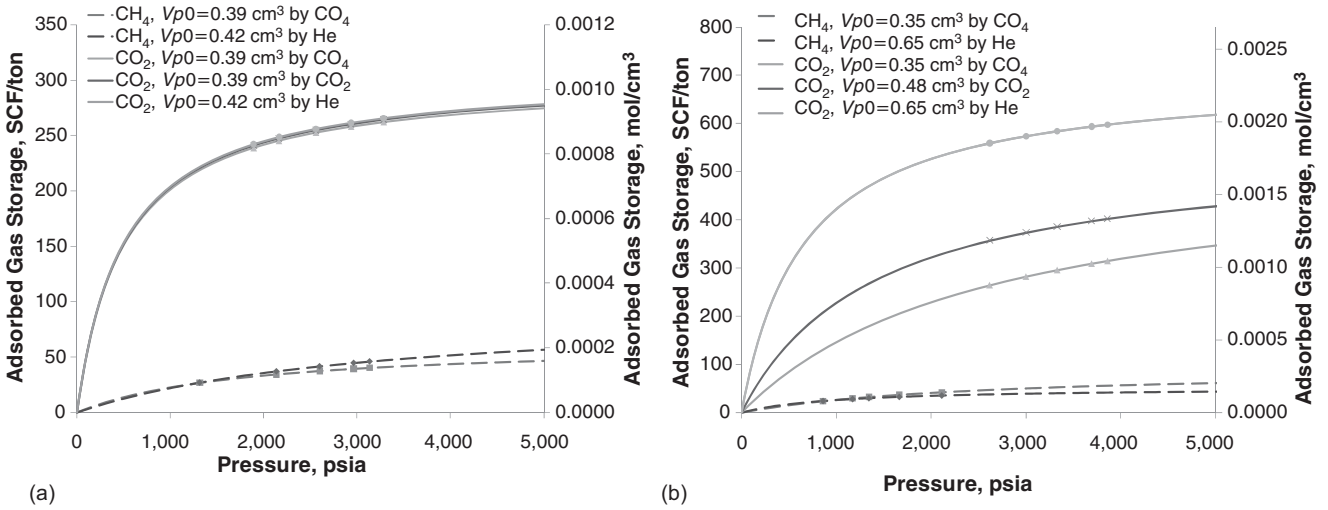

Fig. 8—Estimated Langmuir isotherms for Sample 21 (a) and Sample 23 (b). The parameters used are given in Table 4. The markers show the five experimental pressure data points used during the prediction of the gas-storage parameters.

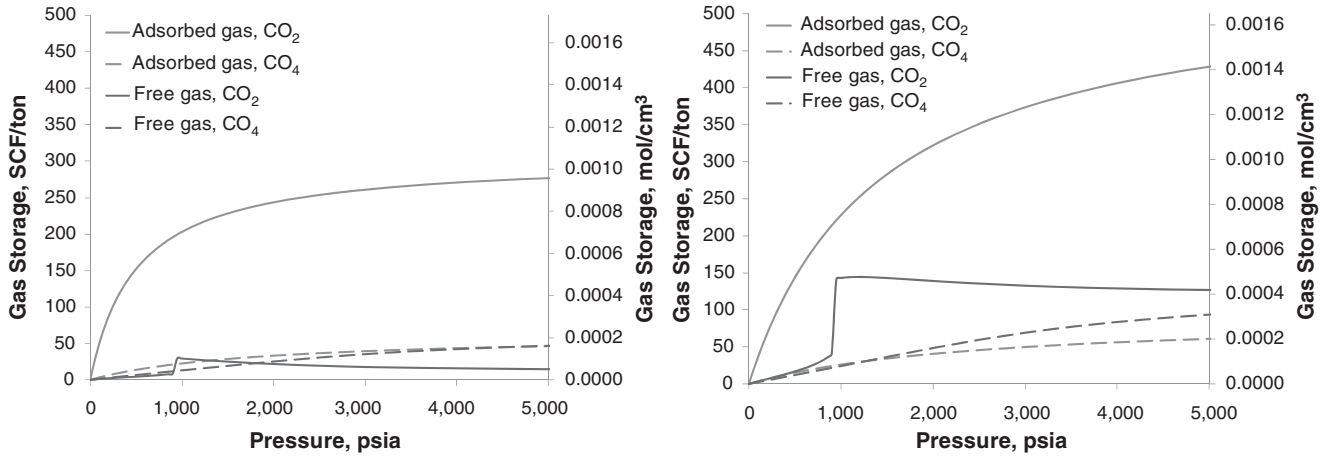

Fig. 9—Estimated adsorbed- and free-gas amounts for Sample 21 (a) and Sample 23 (b). Solid lines are with CO_2, and the dashed lines are with methane.

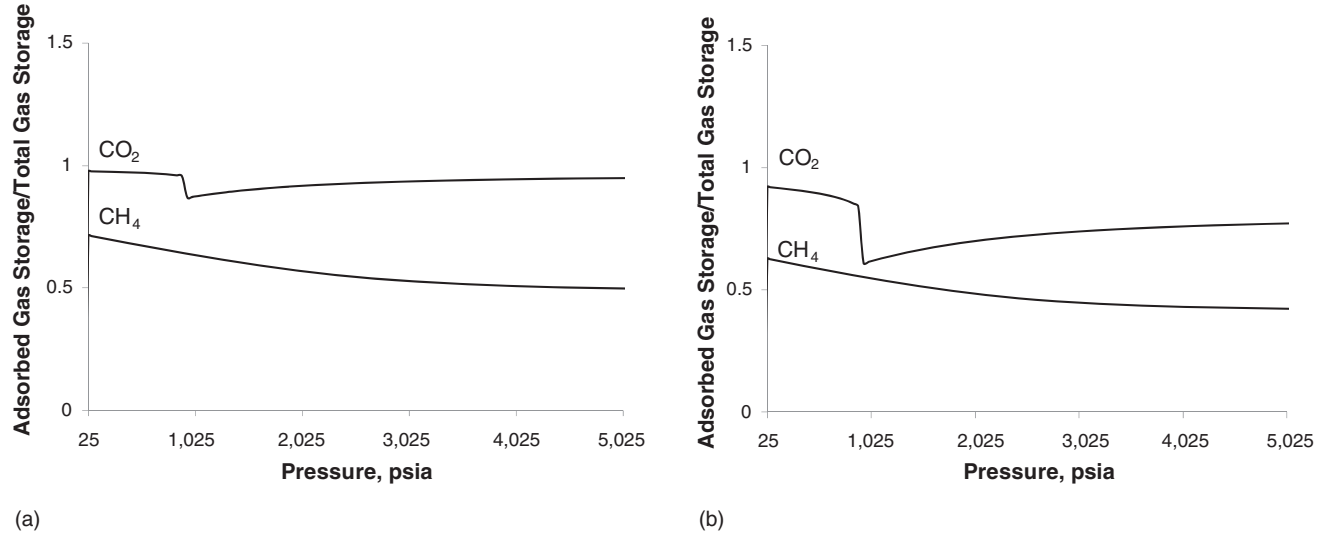

Fig. 10—Estimated ratio of adsorbed gas to total gas stored in Sample 21 (a) and in Sample 23 (b).

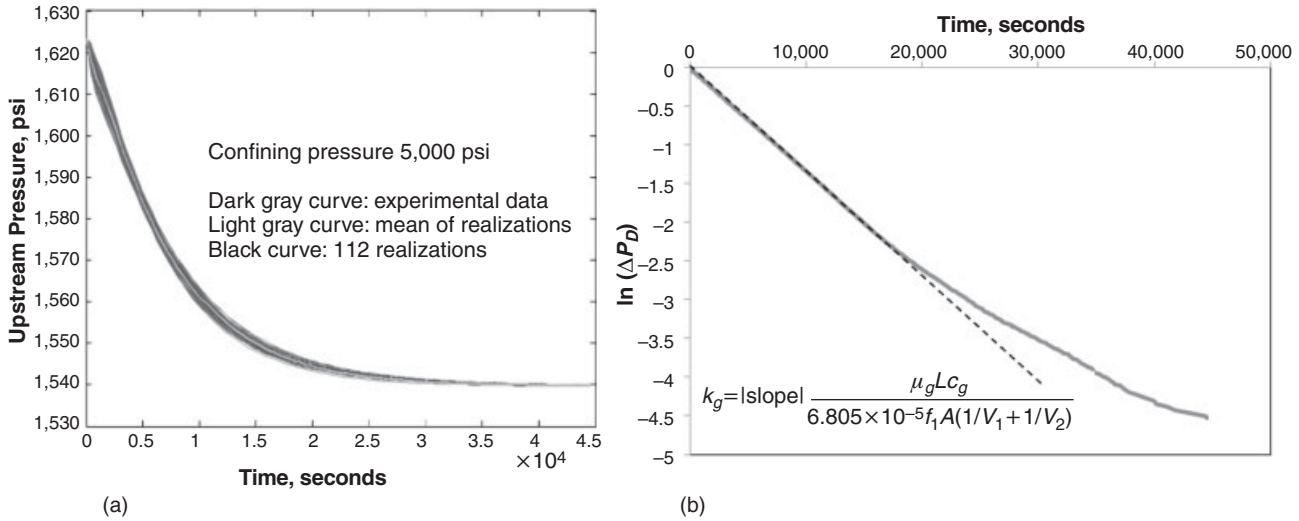

Fig. 11—(a) Example history-matching results for Sample 21 using upstream pressure decline. 112 realizations are used to obtain the optimum values of the transport coefficients shown in the first row in Table 5. (b) Permeability for Sample 21 is obtained using the pulse decay shown on the left and using Jones' straight-line method (Jones 1997).

of adsorbed CO_2 to total CO_2 gas storage is approximately 0.93 for Sample 21; on the other hand, the ratio for methane is approximately 0.54 for the same sample. In the case of Sample 23, at the same pressure, the ratios are 0.72 and 0.46, respectively.

The rapid change in free-gas-CO_2 measurements near 950 psia in Figs. 9 and 10 is caused by dramatic changes in the z factor of the gas near the critical fluid state.

The estimated coefficient of isothermal pore-volume-compressibility values in Table 4 are nearly the same for the two samples, taking values on the order of from 5.0×10^{-6} to 7.0×10^{-6} psi^{-1}. During our gas-storage measurements and calculations, we found that the results would have been less than 5% different when the pore-compressibility effect had been ignored. Thus, the primary correction necessary for the organic pore volume is the adsorption effect. This behavior is quite different than in coals where most of the matrix is organic and the pore-volume-compressibility values could be one or two orders of magnitude larger; hence, its effect on the pore volume measurements in coal becomes comparable to the sorption effects (Koleowo 2010).

Finally, the estimated adsorbed-phase density values in Table 4 for methane and CO_2 are in agreement with those reported in the literature (Kurniawan et al. 2006; Ambrose et al. 2010), indicating that the gas-storage models are reasonable and that the density for the adsorbed-phase is close to the liquid density of the chemical species used during the experiment.

A typical upstream pressure-decline curve of the pulse-decay gas-permeation experiments is shown in **Fig. 11.** In this case, methane initially in equilibrium with shale Sample 21 is allowed to permeate. The curve typically yields two distinct behaviors having completely different characteristic times. At early times, the curve shows a rapid decline in pressure (fast transport), and, later, it slows down, gradually decreasing the upstream pressure (slow transport). These distinct portions of the decline curve include information related to Darcy flow in the inorganic matrix consisting of large voids, and pore/surface diffusion in the organic pore network. In addition, the total time required for the shale/gas system to reach the new thermodynamic equilibrium is related to gas storability for the shale and can be used to obtain basic information such as organic-/inorganic-pore-volume ratio. Having the pressure-decline curve, we used a simulation-based history-matching algorithm based on the randomized maximum likelihood method and estimated the optimized transport properties of the shale samples. The optimization requires different realizations of the parameter space, typically on the order of hundreds. Details of the automated nonlinear history-matching process are described elsewhere (Oliver et al. 2008). Here, salient results related to the nature of multiscale gas transport in shale are discussed for the sequestration. Most importantly, we found that it is not possible to obtain converging (optimum) results using unipore shale-matrix models for the forward simulation; the matrix model used for the history matching should be a dual-porosity (organic/inorganic) system. History-matching results at various confining-stress conditions and using a multiscale transport model are shown in **Table 5** for Samples 21 and 23. Note that the time required to reach the new equilibrium is significantly less as the pore pressure is increased. This indicates that the transport paths are sensitive to effective stress. The observation is supported further by the increase in the estimated inorganic permeability and organic diffusivity values. We note that permeability estimates are significantly less than those obtained using conventional measurements, such as Jones' method (see also Fig. 11b for details). This is possibly because of the explicit introduction of ultralow-permeability organics into the description of shale-gas transport in this work.

It was argued in the Interpretation of Organic Pore Diffusion subsection that the pore-diffusion coefficient for a single capillary should typically be two orders of magnitude larger than the experimentally obtained apparent free-gas transport coefficient D_K. Here, using Eq. 4, we experimentally predict tortuosity values within the range of 4.0 to 6.0 for the kerogen. The estimated values are consistent with the literature, showing high tortuosity values for microporous materials and suggesting that the measured diffusion coefficient indeed represents the coefficient for pore diffusion of free gas. More interestingly, the coefficient for adsorbed-phase transport D_S is predicted to be typically three orders of magnitude larger than that for the free gas. This is a somewhat curious behavior, which suggests that the surface diffusion could be the dominant mechanism of transport in the organics. Typically, the adsorbed-phase concentration and its gradient in the organics are smaller than those values associated with the free gas; however, when multiplied with an extremely large surface diffusivity, the product (i.e., mass flux of the adsorbed phase) becomes a quantity that significantly contributes to the total mass flux in the kerogen. The importance of surface diffusion to the gas transport in heterogeneous coals and shales has been discussed recently by Fathi (2010) and Fathi and Akkutlu (in press) on the basis of theoretical arguments in the spectral (Fourier-Laplace) domain. Here, the experimental results support the observation, suggesting that the sequestered gases will also be transported as part of the adsorbed phase in the organics. **Fig. 12** shows that the estimated mass flux from surface diffusion of the adsorbed gas molecules is comparable to and could be even significantly larger than the mass flux from pore diffusion of the free-gas molecules.

TABLE 5—ESTIMATED METHANE TRANSPORT PARAMETERS* FOR ORGANIC-RICH SHALE SAMPLES USING ISOTHERMAL PULSE-DECAY MEASUREMENTS AT VARYING PORE PRESSURES

Estimated Matrix Parameters for Shale Sample 21

Effective Stress Conditions		Pulse		Total			Inorganic	Kerogen			
Confining Pressure (psi)	Equilibrium Pore Pressure (psi)	p (psi)	Time To Reach Equilibrium (seconds)	Jones' Permeability (nd)	TOC (mass/mass) %	ϕ (vol/vol) %	k (nd)	ε_{k0}	τ	D_K (cm^2/s)	D_S (cm^2/s)
	0					1.73					
5,000	1,623	83	44,485	70.4	3.9	1.33	15.8	53.87	4.45	3.50×10^{-5}	1.10×10^{-2}
5,000	2,588	84	18,063	102.2	3.9	1.24	20.4	64.16	4.39	4.00×10^{-5}	4.20×10^{-2}
5,000	2,974	70	12,060	122.9	3.9	1.22	28.7	67.56	4.04	4.90×10^{-5}	8.80×10^{-2}

Estimated Matrix Parameters for Shale Sample 23

Effective Stress Conditions		Pulse		Total			Inorganic	Kerogen			
Confining Pressure (psi)	Equilibrium Pore Pressure (psi)	p (psi)	Time To Reach Equilibrium (seconds)	Jones' Permeability (nd)	TOC (mass/mass) %	ϕ (vol/vol) %	k (nd)	ε_{k0}	τ	D_K (cm^2/s)	D_S (cm^2/s)
	0					2.85					
5,000	1,772	78	72,060	12.65	3	2.4	2.6	43.58	6.14	3.50×10^{-5}	1.55×10^{-3}
5,000	25,008	74	54,480	16.31	3	2.32	3.52	47.09	5.10	5.30×10^{-5}	3.50×10^{-3}
5,000	3,066	73	32,520	17.7	3	2.27	5.24	48.23	4.10	8.20×10^{-5}	6.35×10^{-3}

* In the tables, porosity represents the void volume available for free gas only; hence, porosity is corrected for the pore compressibility and methane-adsorption effects; TOC is measured independently; ε_{k0} represents the ratio of kerogen pore volume to the total pore volume; D_k is the molecular diffusivity of free gas in kerogen.

Further investigation using different shale samples is currently necessary.

Conclusions

In this paper, we have developed methodologies that allow us to investigate in detail CO_2 sequestration in organic-rich gas-shale samples from Forth Worth basin. It is found that the pore-volume estimation is a crucial step for the sequestration considerations in gas shale. This volume may not be important for the storage of free gas, however, because up to 97% of the uptaken gas is stored in adsorbed state inside the organic pores, depending on the shale-gas-reservoir pressure and temperature. It is also found that the gas transport takes place in the presence of dynamic porosity and permeability, and it could be dominated by the adsorbed-phase transport taking place in the organics. It is a difficult task to experimentally differentiate slippage of free-gas molecules and surface-diffusion effects taking place in the phase-transition region near the organic nanopore walls, although strong dependence on the adsorbed-phase gradient indicates the significance of surface diffusion in the organics. Although the study is important for our understanding of gas storage and transport in organic-rich shale, gas shales in North America may differ in terms of organic content, pore structure of the organic material, and temperature. Further investigation involving samples from different shale plays is necessary for statistical inference and generalization of the results.

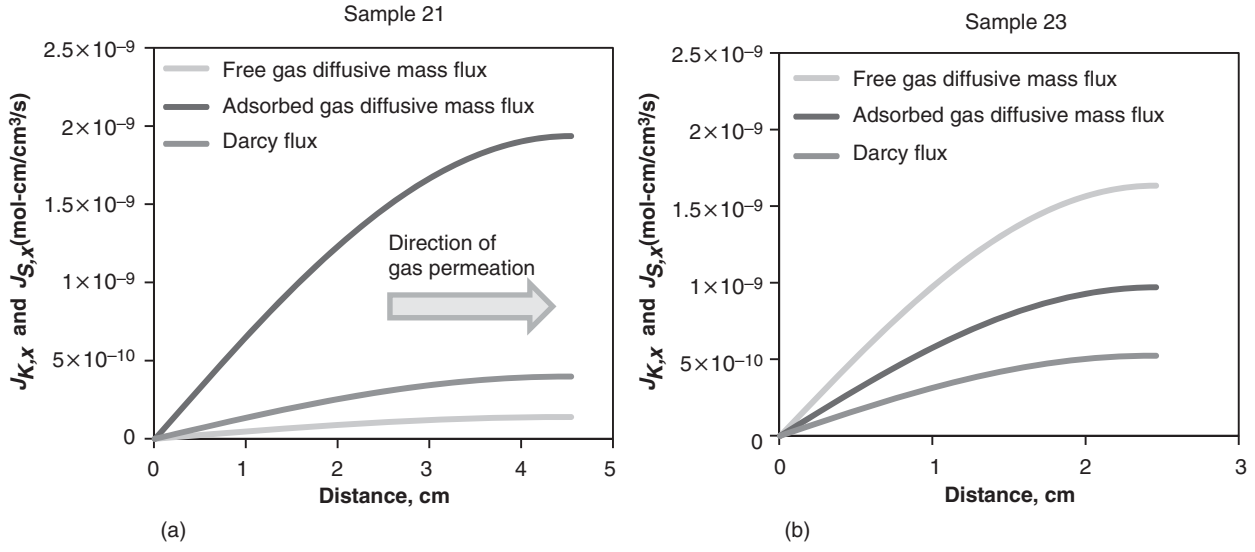

Fig. 12—Predicted mass fluxes across the shale Sample 21 at initial equilibrium pore pressure of 2,974 psia and Sample 23 at 3,066 psia during the pressure-pulse-decay measurements. The mass fluxes are computed using forward simulation with the optimized transport parameters shown in Table 5. Only the flux values at the halftime to reach the new equilibrium pressure during the pulse-decay measurement are shown.

Nomenclature

A_s = surface area, nm^2
C = moles of concentration
C_p = the pore-volume compressibility, psi^{-1}
C_μ = adsorbed-phase amount in moles per solid organic volume, mol/cm^3
D_K = pore-diffusion coefficient, cm^2/s
$D_{K,\text{ capillary}}$ = molecular-diffusion coefficient for gas transport in the capillary, cm^2/s
D_S = porosity- and tortuosity-corrected surface diffusivity, cm^2/s
$J_{K,x}$ = pore-diffusion mass flux, mol·cm/cm^3/s
$J_{S,x}$ = surface-diffusion mass flux, mol·cm/cm^3/s
n = number of moles, mol
n_1 = moles of gas in V_1, mol
n_{1f} = moles of gas in V_1 at P_f, mol
n_2 = moles of gas in V_2, mol
n_{2f} = moles of gas in V_2 at P_f, mol
n_{sp} = moles of gas stored in the sample, mol
N_{Kn} = Knudsen number
P = pore pressure
P_1 = equilibrium pressure in V_1, psia
P_2 = initial pressure in V_3, psia
P_f = new equilibrium pressure in dead volume and sample volume, psia
P_L = Langmuir pressure, psia
P_s = pore pressure in the sample, psia
S_a = adsorbed-gas storage, mol
$S_{a\max}$ = total moles of adsorbed gas at infinite pore pressure, mol
S_w = water saturation, %
V_1 = reservoir volume, cm^3
V_2 = dead volume, cm^3
V_a = adsorbed-gas volume, cm^3
$V_{a\max}$ = maximum adsorbed gas, cm^3
V_L = Langmuir volume, scf/ton
V_p = sample pore volume, cm^3
V_{p0} = pore volume at zero pore pressure, cm^3
V_{p2} = pore volume at P_2, cm^3
V_{pf} = pore volume at P_f, cm^3
z_1 = correction factor at P_1
z_2 = correction factor at P_2
z_f = correction factor at P_f
z_s = correction factor at P_s
Δn_1 = change of moles of gas in V_1, mol
Δn_2 = change of moles of gas in V_2, mol
Δn_s = change of moles of gas in sample, mol
Δn_{sa} = change of moles of adsorbed gas in sample, mol
Δn_{sp} = change of moles of gas stored in sample, mol
ΔV_{pa} = change of volume of adsorbed gas in sample, cm^3
ΔV_{pp} = change of pore volume at the pore pressure in sample, cm^3
ε_{k0} = organic pore volume to total pore volume, ratio
ε_{TOC} = kerogen to total volume ratio
ρ = bulk density of gas, g/cm^3
ρ_{ads} = molar density of adsorbed gas, mole/cm^3
τ = tortuosity
ϕ = porosity

Acknowledgments

We recognize the work and contributions of Gary D. Stowe in the IC^3 laboratory at The University of Oklahoma. We thank Mery Diaz-Campos for her contribution to the generation of Fig. 2. For insightful discussions, we thank Chandra S. Rai and Carl H. Sondergeld in shale petrophysics and Dean S. Oliver in nonlinear optimization.

References

Ambrose, R.J., Hartman, R.C., Diaz-Campos, M., Akkutlu, I.Y., and Sondergeld, C.H. 2010. New Pore-scale Considerations in Shale Gas in Place Calculations. Paper SPE 131772 presented at the SPE Unconventional Gas Conference, Pittsburgh, Pennsylvania, 23–25 February. doi: 10.2118/131772-MS.

Anderson, J.R. and Pratt, K.C. 1985. *Introduction to Characterization and Testing of Catalysts*. Sydney, Australia: Academic Press.

Bear, J. and Bachmat, Y. 1991. *Introduction to Modeling of Transport Phenomena in Porous Media*, paperback edition. Dordrecht, The Netherlands: Theory and Applications of Transport in Porous Media, Kluwer Academic Publishers.

Brace, W.F., Walsh, J.B., and Frangos, W.T. 1968. Permeability of Granite Under High Pressure. *J. Geophys. Res.* **73** (6): 2225–2236. doi: 10.1029/JB073i006p02225.

Busch, A., Alles, S., Gensterblum, Y., Prinz, D., Dewhurst, D.N., Raven, M.D., Stanjek, H., and Krooss, B.M. 2008. Carbon Dioxide Storage Potential of Shales. *International Journal of Greenhouse Gas Control* **2** (3): 297–308. doi: 10.1016/j.ijggc.2008.03.003.

Fathi, E. 2010. Fluid Flow, Transport and Reaction in Heterogeneous Porous Media. PhD thesis, University of Oklahoma, Norman, Oklahoma.

Fathi, E. and Akkutlu, I.Y. 2009. Matrix Heterogeneity Effects on Gas Transport and Adsorption in Coalbed and Shale Gas Reservoirs. *Transport in Porous Media* **80** (2): 281–304. doi: 10.1007/s11242-009-9359-4.

Fathi, E. and Akkutlu, I.Y. *In press*. Mass Transport of Adsorbed-phase in Stochastic Porous Medium with Fluctuating Porosity Field and Nonlinear Gas Adsorption Kinetics. *Transport in Porous Media* (submitted 2010).

Finsterle, S. and Persoff, P. 1997. Determining Permeability of Tight Rock Samples Using Inverse Modeling. *Water Resour. Res.* **33** (8): 1803–1811.

Jones, S.C. 1997. A Technique for Faster Pulse-Decay Permeability Measurements in Tight Rocks. *SPE Form Eval* **12** (1): 19–26. SPE- 28450-PA. doi: 10.2118/28450-PA.

Koleowo, O.B. 2010. Gas Storage Capacity and Transport in Coals. MS thesis, University of Oklahoma, Norman, Oklahoma.

Kurniawan, Y., Bhatia, S.K., and Rudolph, V. 2006. Simulation of Binary Mixture Adsorption of Methane and CO_2 at Supercritical Conditions in Carbons. *AIChE Journal* **52** (3): 957–967. doi: 10.1002/aic.10687.

Lee, B. and Tan, T. 1987. Application of Multiple Porosity/Permeability Simulator in Fractured Reservoir Simulation. Paper SPE 16009 presented at the SPE Symposium on Reservoir Simulation, San Antonio, Texas, USA, 1–4 February. doi: 10.2118/16009-MS.

Loucks, R.G., Reed, R.M., Ruppel, S.C., and Jarvie, D.M. 2009. Morphology, Genesis, and Distribution of Nanometer-Scale Pores in Siliceous Mudstones of the Mississippian Barnett Shale. *Journal of Sedimentary Research* **79** (12): 848–861. doi: 10.2110/jsr.2009.092.

Ning, X. 1992. The Measurement of Matrix and Fracture Properties in Naturally Fractured Low Permeability Cores using a Pressure Pulse Method. PhD thesis, Texas A&M University, College Station, Texas.

Ozdemir, E., Morsi, B.I., and Schroeder, K. 2004. CO_2 Adsorption Capacity of Argonne Premium Coals. *Fuel* **83** (7–8): 1085–1094.

Oliver, D.S., Reynolds, A.C., and Liu, N. 2008. *Inverse Theory for Petroleum Reservoir Characterization and History Matching.* Cambridge University Press.

Roy, S., Raju, R., Chuang, H.F., Cruden, B.A., and Meyyappan, M. 2003. Modeling Gas Flow Through Microchannels and Nanopores. *J. Appl. Phys.* **93** (8): 4870–4879. doi: 10.1063/1.1559936.

Schettler, P.D., Parmely, C.R., Juniata, C., and Lee, W.J. 1989. Gas Storage and Transport in Devonian Shales. *SPE Form Eval* **4** (3): 371–376; *Trans.,* AIME, **287**. SPE-17070-PA. doi: 10.2118/17070-PA.

Sondergeld, C.H., Ambrose, R.J., Rai, C.S., and Moncrieff, J. 2010. Micro-Structural Studies of Gas Shales. Paper SPE 131771 presented at the SPE Unconventional Gas Conference, Pittsburg, Pennsylvania, USA, 23–25 February 2010. doi: 10.2118/131771-MS.

Wang, F.P. and Reed, R.M. 2009. Pore Networks and Fluid Flow in Gas Shales. Paper SPE 124253 presented at the SPE Annual Technical Conference and Exhibition, New Orleans, 4–7 October. doi: 10.2118/124253-MS.

Wei, X.R., Weng, G.X., Massarotto, P., Rudolph, V., and Golding, S.D. 2007. Modeling Gas Displacement Kinetics in Coal With Maxwell-Stefan Diffusion Theory. *AIChE Journal* **53** (12): 3241–3252. doi: 10.1002/aic.11314.

Seung Mo Kang is an MS student in petroleum engineering at The University of Oklahoma. He holds a BS degree in mechanical engineering from Hanyang University in South Korea. His current research interest is quantification of gas-storage mechanisms in shale gas reservoirs. **Ebrahim Fathi** is a research associate at The University of Oklahoma. Fathi holds BS and MS degrees in exploration of mining and petroleum engineering from Tehran University. He holds a PhD degree in petroleum engineering from The University of Oklahoma. His research interests are up-scaling of the fluid flow, transport and reaction processes in heterogeneous porous media, gas transport and storage in shale gas and coalbed methane reservoirs, and simulation of flow dynamics in naturally occurring nanoporous materials. **Raymond J. Ambrose** is a PhD student in petroleum engineering at The University of Oklahoma and director of reservoir engineering for Reliance Holding USA. He holds a BS degree in chemical engineering and an MS degree in petroleum engineering, both from the University of Southern California. His current research interests are analytical solutions for gas shale productivity, SEM imaging and pore structure characterization for organic-rich gas shale, identification of gas-storage mechanisms in unconventional gas resources, and estimation of gas in place. **I. Yucel Akkutlu** is professor of petroleum engineering at The University of Oklahoma. He holds MS and PhD degrees from the University of Southern California. His work finds applications in reservoir engineering, particularly in the areas of unconventional gas recovery and improved and enhanced oil recovery. His current research deals with the thermodynamics of fluids in nanoporous materials and with the scaling up of coupled transport and reaction processes in low-permeability geological formations exhibiting multiscale pore structures. **Richard F. Sigal** joined The University of Oklahoma in 2004 as Unocal Centennial Professor with a joint appointment in petroleum engineering and geology and geophysics. His primary research activity since then has been on tight gas, shale gas, and other unconventional gas reservoirs. Before joining The University of Oklahoma, he worked in the oil and gas industry for 26 years on reservoir characterization, core measurements, and petrophysics. Among his areas of special expertise are nuclear magnetic resonance, mercury capillary pressure measurements, and the stress dependence of permeability.